

Constrained Deep Networks: Lagrangian Optimization via Log-Barrier Extensions

Hoel Kervadec, Jose Dolz, Jing Yuan, Christian Desrosiers, Eric Granger, Ismail Ben Ayed

Abstract—This study investigates imposing inequality constraints on the outputs of CNNs, with application to weakly supervised segmentation. In the context of deep networks, constraints are commonly handled with *penalties* for their simplicity, and despite their well-known limitations. Lagrangian-dual optimization has been largely avoided, mainly due to the computational complexity and stability/convergence issues caused by alternating *explicit* dual updates/projections and stochastic optimization. Several studies showed that, for deep CNNs, the theoretical and practical advantages of Lagrangian optimization over penalties do not materialize in practice. We propose *log-barrier extensions*, which approximate Lagrangian optimization of constrained-CNN problems with a sequence of unconstrained losses. Unlike standard interior-point and log-barrier methods, our formulation does not need an initial feasible solution. Furthermore, we provide a new technical result, which shows that the proposed extensions yield an upper bound on the duality gap. This generalizes the duality-gap result of standard log-barriers, yielding sub-optimality certificates for feasible solutions. While sub-optimality is not guaranteed for non-convex problems, our result shows that log-barrier extensions are a principled way to approximate Lagrangian optimization for constrained CNNs via *implicit* dual variables. We report comprehensive constrained-CNN experiments, showing that our formulation outperforms several penalty-based methods, in terms of accuracy and training stability.

Index Terms—Log-barrier extensions, Lagrangian optimization, Constraints, CNNs, deep networks, weakly supervised segmentation.

1 INTRODUCTION

DEEP convolutional neural networks (CNNs) are dominating in most visual recognition problems and applications, including semantic segmentation [19], action recognition [30] and object detection [6], among many others. When full supervision is available, CNNs can achieve outstanding performances, but this type of supervision may not be available in a breadth of applications. In semantic segmentation, for instance, full supervision involves annotating all the pixels in each training image. The problem is further amplified when such annotations require expert knowledge or involves volumetric data, as is the case in medical imaging [18]. Therefore, the supervision of semantic segmentation with partial or weak labels, for example, scribbles [16], [32], [33], image tags [23], [26], bounding boxes [27] or points [1], has received significant research efforts in the last years.

Imposing prior knowledge on the network’s prediction via some unsupervised loss is a well-established technique in semi-supervised learning [7], [35]. Such a prior acts as a regularizer that leverages unlabeled data with domain-specific knowledge. For instance, in semantic segmentation, several recent works showed that adding loss terms such as dense conditional random fields (CRFs) [20], [33], graph clustering [32] or priors on the sizes of the target regions [14], [15], [37] can achieve outstanding performances with only fractions of full supervision labels. However, imposing hard inequality or equality constraints on the output of deep CNNs is still in a nascent stage, and only a few recent works have focused on the subject [15], [21], [26], [28].

1.1 Problem formulation

We consider a general class of semi- or weakly-supervised semantic segmentation problems, where *global inequality constraints* are enforced on the network’s output. Consider a training image $I : \Omega \subset \mathbb{R}^2 \rightarrow \mathbb{R}$, with $\Omega_{\mathcal{L}} \subset \Omega$ a set of labeled pixels, which corresponds to a fraction of the pixels in image domain Ω . For K classes, let $\mathbf{y}_p = (y_p^1, \dots, y_p^K) \in \{0, 1\}^K$ denotes the ground-truth label of pixel $p \in \Omega_{\mathcal{L}}$, and $S_{\theta} \in [0, 1]^{|\Omega| \times K}$ a standard K -way softmax probability output, with θ the network’s parameters. In matrix S_{θ} , each row $\mathbf{s}_{p,\theta} = (s_{p,\theta}^1, \dots, s_{p,\theta}^K) \in [0, 1]^K$ corresponds to the predictions for a pixel p in Ω , which can be either unlabeled or labeled. We focus on constrained problems of the following general form:

$$\begin{aligned} \min_{\theta} \mathcal{E}(\theta) \\ \text{s.t. } f_i(S_{\theta}) \leq 0, \quad i = 1, \dots, N \end{aligned} \quad (1)$$

where $\mathcal{E}(\theta)$ is some standard loss for labeled pixels $p \in \Omega_{\mathcal{L}}$, e.g., the cross entropy¹: $\mathcal{E}(\theta) = -\sum_{p \in \Omega_{\mathcal{L}}} \sum_k y_p^k \log(s_{p,\theta}^k)$. Inequality constraints of the general form in (1) can embed very useful prior knowledge on the network’s predictions for unlabeled pixels. Assume, for instance, that we have prior knowledge about the size of the target region (i.e., class) k . Such a knowledge can be in the form of lower or upper bounds on region size, which is common in medical image segmentation problems [8], [15], [22]. In this case, one can impose constraints of the form $f_i(S_{\theta}) = \sum_{p \in \Omega} s_{p,\theta}^k - a$, with a denoting an upper bound on the size of region k . The same type of constraints can impose image-tag priors, a form of weak supervision enforcing whether a target region is present or absent in a given training image, as in multiple instance learning (MIL) scenarios [15], [26]. For instance,

1. We give the cross entropy as an example but our framework is not restricted to a specific form of loss for the set of labeled points.

• H. Kervadec, J. Dolz, C. Desrosiers, E. Granger and I. Ben Ayed are with ETS Montreal, Canada
 • J. Yuan is with the School of Math. and Stat., Xidian University, China.

constraint of the form $f_i(S_\theta) = 1 - \sum_{p \in \Omega} s_{p,\theta}^k$ forces class k to be present in a given training image.

1.2 Challenges of constrained CNN optimization

As pointed out in several recent studies [15], [21], [26], imposing hard constraints on deep CNNs involving millions of trainable parameters is challenging. This is the case of problem (1), even when the constraints are convex with respect to the outputs of the network. In optimization, a standard way to handle constraints is to solve the Lagrangian primal and dual problems in an alternating scheme [3]. For (1), this corresponds to alternating the optimization of a CNN for the primal with stochastic optimization, e.g., SGD, and projected gradient-ascent iterates for the dual. However, despite the clear benefits of imposing global constraints on CNNs, such a standard Lagrangian-dual optimization is mostly avoided in modern deep networks. As discussed recently in [21], [26], [28], this might be explained by the computational complexity and stability/convergence issues caused by alternating between stochastic optimization and dual updates/projections.

In standard Lagrangian-dual optimization, an unconstrained problem needs to be solved after each iterative dual step. This is not feasible for deep CNNs, however, as it would require re-training the network at each step. To avoid this problem, Pathak et al. [26] introduced a latent distribution, and minimized a KL divergence so that the CNN output matches this distribution as closely as possible. Since the network’s output is not directly coupled with constraints, its parameters can be optimized using standard techniques like SGD. While this strategy enabled adding inequality constraints in weakly supervised segmentation, it is limited to linear constraints. Moreover, the work in [21] imposed hard equality constraints on 3D human pose estimation. To alleviate the ensuing computational complexity, they used a Kyrlov sub-space approach, limiting the solver to a randomly selected subset of constraints within each iteration. Therefore, constraints that are satisfied at one iteration may not be satisfied at the next, which might explain the negative results obtained in [21]. In general, updating the network parameters and dual variables in an alternating fashion leads to a higher computational complexity than solving a loss function directly.

Another important difficulty in Lagrangian optimization is the interplay between stochastic optimization (e.g., SGD) for the primal and the iterates/projections for the dual. Basic gradient methods have well-known issues with deep networks, e.g., they are sensitive to the learning rate and prone to weak local minima. Therefore, the dual part in Lagrangian optimization might obstruct the practical and theoretical benefits of stochastic optimization (e.g., speed and strong generalization performance), which are widely established for unconstrained deep network losses [10]. More importantly, solving the primal and dual separately may lead to instability during training or slow convergence, as shown recently in [15].

1.3 Penalty approaches

In the context of deep networks, “hard” inequality or equality constraints are typically handled in a “soft” manner by augmenting the loss with a *penalty* function [11], [13], [15]. Such a penalty approach is a simple alternative to Lagrangian optimization, and is well-known in the general context of constrained optimization;

see [2], Chapter 4. In general, penalty-based methods approximate a constrained minimization problem with an unconstrained one by adding a term (penalty) $\mathcal{P}(f_i(S_\theta))$, which increases when constraint $f_i(S_\theta) \leq 0$ is violated. By definition, a penalty \mathcal{P} is a non-negative, continuous and differentiable function, which verifies: $\mathcal{P}(f_i(S_\theta)) = 0$ if and only if constraint $f_i(S_\theta) \leq 0$ is satisfied. In semantic segmentation [15] and, more generally, in deep learning [11], it is common to use a quadratic penalty for imposing an inequality constraint: $\mathcal{P}(f_i(S_\theta)) = [f_i(S_\theta)]_+^2$, where $[x]_+ = \max(0, x)$ denotes the rectifier function. Fig. 1 depicts different penalty functions. Penalties are convenient for deep networks because they remove the requirement for explicit Lagrangian-dual optimization. The inequality constraints are fully handled within stochastic optimization, as in standard unconstrained losses, avoiding gradient ascent iterates/projections over the dual variables and reducing the computational load for training [15]. However, this simplicity of penalty methods comes at a price. In fact, it is well known that penalties do not guarantee constraint satisfaction and require careful and *ad hoc* tuning of the relative importance (or weight) of each penalty term in the overall function. More importantly, in the case of several competing constraints, penalties do not act as *barriers* at the boundary of the feasible set (i.e., a satisfied constraint yields a null penalty and null gradient). As a result, a subset of constraints that are satisfied at one iteration may not be satisfied at the next. Take the case of two competing constraints f_1 and f_2 at the current iteration (assuming gradient-descent optimization), and suppose that f_1 is satisfied but f_2 is not. The gradient of a penalty \mathcal{P} w.r.t the term of satisfied constraint f_1 is null, and the the penalty approach will focus solely on satisfying f_2 . Therefore, due to a null gradient, there is nothing that prevents satisfied constraint f_1 from being violated. This could lead to oscillations between competing constraints during iterations, making the training unstable (we will give examples in the experiments).

Lagrangian optimization can deal with these difficulties, and has several well-known theoretical and practical advantages over penalty methods [4], [5]: it finds automatically the optimal weights of the constraints, acts as a barrier for satisfied constraints and guarantees constraint satisfaction when feasible solutions exist. Unfortunately, as pointed out recently in [15], [21], these advantages of Lagrangian optimization do not materialize in practice in the context of deep CNNs. Apart from the computational-feasibility aspects, which the recent works in [21], [26] address to some extent with approximations, the performances of Lagrangian optimization are, surprisingly, below those obtained with simple, much less computationally intensive penalties [15], [21]. This is, for instance, the case of the recent weakly supervised CNN semantic segmentation results in [15], which showed that a simple quadratic-penalty formulation of inequality constraints outperforms substantially the Lagrangian method in [26]. Also, the authors of [21] reported surprising results in the context of 3D human pose estimation. In their case, replacing the equality constraints with simple quadratic penalties yielded better results than Lagrangian optimization.

1.4 Contributions

Interior-point and log-barrier methods can approximate Lagrangian optimization by starting from a feasible solution and solving unconstrained problems, while completely avoiding explicit dual steps and projections. Unfortunately, despite their

well-established advantages over penalties, such standard log-barriers were not used before in deep CNNs because finding a feasible set of initial network parameters is not trivial, and is itself a challenging constrained-CNN problem. We propose *log-barrier extensions*, which approximate Lagrangian optimization of constrained-CNN problems with a sequence of unconstrained losses, without the need for an initial feasible set of network parameters. Furthermore, we provide a new theoretical result, which shows that the proposed extensions yield a duality-gap bound. This generalizes the standard duality-gap result of log-barriers, yielding sub-optimality certificates for feasible solutions in the case of convex losses. While sub-optimality is not guaranteed for non-convex problems, our result shows that log-barrier extensions are a principled way to approximate Lagrangian optimization for constrained CNNs via *implicit* dual variables. Our approach addresses the well-known limitations of penalty methods and, at the same time, removes the explicit dual updates of Lagrangian optimization. We report comprehensive experiments showing that our formulation outperforms various penalty-based methods for constrained CNNs, both in terms of accuracy and training stability.

2 BACKGROUND ON LAGRANGIAN-DUAL OPTIMIZATION AND THE STANDARD LOG-BARRIER

This section reviews both standard Lagrangian-dual optimization and the log-barrier method for constrained problems [3]. We also present basic concepts of duality theory, namely the *duality gap* and ϵ -suboptimality, which will be needed when introducing our log-barrier extension and the corresponding duality-gap bound. We also discuss the limitations of standard constrained optimization methods in the context of deep CNNs.

Lagrangian-dual optimization: Let us first examine standard Lagrangian optimization for problem (1):

$$\mathcal{L}(S_{\theta}, \boldsymbol{\lambda}) = \mathcal{E}(\boldsymbol{\theta}) + \sum_{i=1}^N \lambda_i f_i(S_{\theta}) \quad (2)$$

where $\boldsymbol{\lambda} = (\lambda_1, \dots, \lambda_N)$ is the dual variable (or Lagrange-multiplier) vector, with λ_i the multiplier associated with constraint $f_i(S_{\theta}) \leq 0$. The dual function is the minimum value of Lagrangian (2) over $\boldsymbol{\theta}$: $g(\boldsymbol{\lambda}) = \min_{\boldsymbol{\theta}} \mathcal{L}(S_{\theta}, \boldsymbol{\lambda})$. A dual feasible $\boldsymbol{\lambda} \geq 0$ yields a lower bound on the optimal value of constrained problem (1), which we denote \mathcal{E}^* : $g(\boldsymbol{\lambda}) \leq \mathcal{E}^*$. This important inequality can be easily verified, even when the problem (1) is not convex; see [3], p. 216. It follows that a dual feasible $\boldsymbol{\lambda}$ gives a sub-optimality certificate for a given feasible point $\boldsymbol{\theta}$, without knowing the exact value of \mathcal{E}^* : $\mathcal{E}(\boldsymbol{\theta}) - \mathcal{E}^* \leq \mathcal{E}(\boldsymbol{\theta}) - g(\boldsymbol{\lambda})$. Nonnegative quantity $\mathcal{E}(\boldsymbol{\theta}) - g(\boldsymbol{\lambda})$ is the duality gap for primal-dual pair $(\boldsymbol{\theta}, \boldsymbol{\lambda})$. If we manage to find a feasible primal-dual pair $(\boldsymbol{\theta}, \boldsymbol{\lambda})$ such that the duality gap is less or equal than a certain ϵ , then primal feasible $\boldsymbol{\theta}$ is ϵ -suboptimal.

Definition 1. A primal feasible point $\boldsymbol{\theta}$ is ϵ -suboptimal when it verifies: $\mathcal{E}(\boldsymbol{\theta}) - \mathcal{E}^* \leq \epsilon$.

This provides a non-heuristic stopping criterion for Lagrangian optimization, which alternates two iterative steps, one primal and one dual, each decreasing the duality gap until a given accuracy ϵ is attained². In the context of CNNs [26], the pri-

2. Strong duality should hold if we want to achieve arbitrarily small tolerance ϵ . Of course, strong duality does not hold in the case of CNNs as the primal problem is not convex.

mal step minimizes the Lagrangian w.r.t. $\boldsymbol{\theta}$, which corresponds to training a deep network with stochastic optimization, e.g., SGD: $\arg \min_{\boldsymbol{\theta}} \mathcal{L}(S_{\theta}, \boldsymbol{\lambda})$. The dual step is a constrained maximization of the dual function³ via projected gradient ascent: $\max_{\boldsymbol{\lambda}} g(\boldsymbol{\lambda})$ s.t. $\boldsymbol{\lambda} \geq 0$. As mentioned before, direct use of Lagrangian optimization for deep CNNs increases computational complexity and can lead to instability or poor convergence due to the interplay between stochastic optimization for the primal and the iterates/projections for the dual. Our work approximates Lagrangian-dual optimization with a sequence of unconstrained log-barrier-extension losses, in which the dual variables are *implicit*, avoiding explicit dual iterates/projections. Let us first review the standard log-barrier method.

The standard log-barrier: The log-barrier method is widely used for inequality-constrained optimization, and belongs to the family of *interior-point* techniques [3]. To solve our constrained CNN problem (1) with this method, we need to find a strictly feasible set of network parameters $\boldsymbol{\theta}$ as a starting point, which can then be used in an unconstrained problem via the standard log-barrier function. In the general context of optimization, log-barrier methods proceed in two steps. The first, often called *phase I* [3], computes a feasible point by Lagrangian minimization of a constrained problem, which in the case of (1) is:

$$\begin{aligned} \min_{x, \boldsymbol{\theta}} \quad & x \\ \text{s.t.} \quad & f_i(S_{\boldsymbol{\theta}}) \leq x, \quad i = 1, \dots, N \end{aligned} \quad (3)$$

For deep CNNs with millions of parameters, Lagrangian optimization of problem (3) has the same difficulties as with the initial constrained problem in (1). To find a feasible set of network parameters, one needs to alternate CNN training and projected gradient ascent for the dual variables. This might explain why such interior-point methods, despite their substantial impact in optimization [3], are mostly overlooked in modern deep networks⁴, as is generally the case for other Lagrangian-dual optimization methods.

The second step, often referred to as *phase II*, approximates (1) as an unconstrained problem:

$$\min_{\boldsymbol{\theta}} \mathcal{E}(\boldsymbol{\theta}) + \sum_{i=1}^N \psi_t(f_i(S_{\boldsymbol{\theta}})) \quad (4)$$

where ψ_t is the log-barrier function: $\psi_t(z) = -\frac{1}{t} \log(-z)$. When $t \rightarrow +\infty$, this convex, continuous and twice-differentiable function approaches a hard indicator for the constraints: $H(z) = 0$ if $z \leq 0$ and $+\infty$ otherwise; see Fig. 1 (a) for an illustration. The domain of the function is the set of feasible points. The higher t , the better the quality of the approximation. This suggest that large t yields a good approximation of the initial constrained problem in (1). This is, indeed, confirmed with the following standard duality-gap result for the log-barrier method [3], which shows that optimizing (4) yields a solution that is N/t -suboptimal.

Proposition 1. Let $\boldsymbol{\theta}^*$ be the feasible solution of unconstrained problem (4) and $\boldsymbol{\lambda}^* = (\lambda_1^*, \dots, \lambda_N^*)$, with $\lambda_i^* = -1/(t f_i(S_{\boldsymbol{\theta}^*}))$.

3. Notice that the dual function is always concave as it is the minimum of a family of affine functions, even when the original (or primal) problem is not convex, as is the case for CNNs.

4. Interior-point methods were investigated for artificial neural networks before the deep learning era [34].

Then, the duality gap associated with primal feasible θ^* and dual feasible λ^* for the initial constrained problem in (1) is:

$$\mathcal{E}(\theta^*) - g(\lambda^*) = N/t$$

Proof: The proof can be found in [3], p. 566. \square

An important implication that follows immediately from proposition (1) is that a feasible solution of approximation (4) is N/t -suboptimal: $\mathcal{E}(\theta^*) - \mathcal{E}^* \leq N/t$. This suggests a simple way for solving the initial constrained problem with a guaranteed ϵ -suboptimality: We simply choose large $t = N/\epsilon$ and solve unconstrained problem (4). However, for large t , the log-barrier function is difficult to minimize because its gradient varies rapidly near the boundary of the feasible set. In practice, log-barrier methods solve a sequence of problems of the form (4) with an increasing value t . The solution of a problem is used as a starting point for the next, until a specified ϵ -suboptimality is reached.

3 LOG-BARRIER EXTENSIONS

We propose the following unconstrained loss for approximating Lagrangian optimization of constrained problem (1):

$$\min_{\theta} \mathcal{E}(\theta) + \sum_{i=1}^N \tilde{\psi}_t(f_i(S_{\theta})) \quad (5)$$

where $\tilde{\psi}_t$ is our *log-barrier extension*, which is convex, continuous and twice-differentiable:

$$\tilde{\psi}_t(z) = \begin{cases} -\frac{1}{t} \log(-z) & \text{if } z \leq -\frac{1}{t^2} \\ tz - \frac{1}{t} \log(\frac{1}{t^2}) + \frac{1}{t} & \text{otherwise} \end{cases} \quad (6)$$

Similarly to the standard log-barrier, when $t \rightarrow +\infty$, our extension (6) can be viewed a smooth approximation of hard indicator function H ; see Fig. 1 (b). However, a very important difference is that the domain of our extension $\tilde{\psi}_t$ is not restricted to feasible points θ . Therefore, our approximation (5) removes completely the requirement for explicit Lagrangian-dual optimization for finding a feasible set of network parameters. In our case, the inequality constraints are fully handled within stochastic optimization, as in standard unconstrained losses, avoiding completely gradient ascent iterates and projections over *explicit* dual variables. As we will see in the experiments, our formulation yields better results in terms of accuracy and stability than the recent penalty constrained CNN method in [15].

In our approximation in (5), the Lagrangian dual variables for the initial inequality-constrained problem of (1) are *implicit*. We prove the following duality-gap bound, which yields sub-optimality certificates for feasible solutions of our approximation in (5). Our result⁵ can be viewed as an extension of the standard result in proposition 1, which expresses the duality-gap as a function of t for the log-barrier function.

Proposition 2. *Let θ^* be the solution of problem (5) and $\lambda^* = (\lambda_1^*, \dots, \lambda_N^*)$ the corresponding vector of implicit Lagrangian dual variables given by:*

$$\lambda_i^* = \begin{cases} -\frac{1}{tf_i(S_{\theta^*})} & \text{if } f_i(S_{\theta^*}) \leq -\frac{1}{t^2} \\ t & \text{otherwise} \end{cases}. \quad (7)$$

5. Our result applies to the general context of convex optimization. In deep CNNs, of course, a feasible solution of our approximation may not be unique and is not guaranteed to be a global optimum as \mathcal{E} and the constraints are not convex.

Then, we have the following upper bound on the duality gap associated with primal θ^* and implicit dual feasible λ^* for the initial inequality-constrained problem (1):

$$\mathcal{E}(\theta^*) - g(\lambda^*) \leq N/t$$

Proof: We give a detailed proof of Prop. 2 in the Appendix. \square

From proposition 2, the following important fact follows immediately: If the solution θ^* that we obtain from unconstrained problem (5) is feasible and global, then it is N/t -suboptimal for constrained problem (1): $\mathcal{E}(\theta^*) - \mathcal{E}^* \leq N/t$.

Finally, we arrive to our constrained CNN learning algorithm, which is fully based on SGD. Similarly to the standard log-barrier algorithm, we use a varying parameter t . We optimize a sequence of losses of the form (5) and increase gradually the value t by a factor μ . The network parameters obtained for the current t and epoch are used as a starting point for the next t and epoch. Steps of the proposed constrained CNN learning algorithm are detailed in Algorithm 1.

On the fundamental differences between our log-barrier extensions and penalties: It is important to note that making the log-barrier extension gradually harder by increasing parameter t is not a crucial difference between our formulation and standard penalties. In fact, we can also make standard penalties stricter with a similar gradual increase of t (we will present experiments on this in the next section). The fundamental differences are:

- A penalty does not act as a barrier near the boundary of the feasible set, i.e., a satisfied constraint yields null penalty and gradient. Therefore, at a given gradient update, there is nothing that prevents a satisfied constraint from being violated, causing oscillations between competing constraints and making the training unstable; See Figs. 3 (a) and (d) for an illustration. On the contrary, the strictly positive gradient of our log-barrier extension gets higher when a satisfied constraint approaches violation during optimization, pushing it back towards the feasible set.
- Another fundamental difference is that the derivatives of our log-barrier extensions yield the implicit dual variables in Eq. (7), with sub-optimality and duality-gap guarantees, which is not the case for penalties. Therefore, our log-barrier extension mimics Lagrangian optimization, but with implicit rather than explicit dual variables. The detailed proof of Prop. 2 in the Appendix clarifies how the λ_i^* 's in Eq. (7) can be viewed as implicit dual variables.

Algorithm 1: Log-barrier-extension training for constrained CNNs

Given initial non-strictly feasible $\theta, t := t^{(0)} > 0, \mu > 1$

Repeat (for n epochs)

 Compute $\theta^*(t)$ by minimizing (5) via SGD, starting at

θ

 Update θ . $\rightarrow \theta := \theta^*(t)$

 Increase t . $\rightarrow t := \mu t$

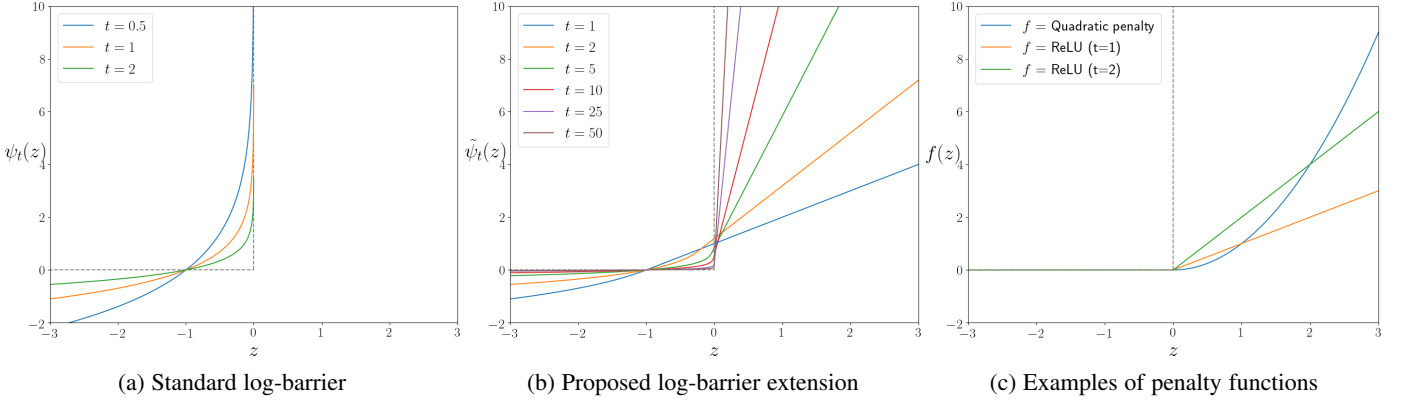


Fig. 1: A graphical illustration of the standard log-barrier in (a), the proposed log-barrier extension in (b) and several examples of penalty functions in (c). The solid curves in colors illustrate several values of t for functions $\psi_t(z)$, $\tilde{\psi}_t(z)$ and the ReLU penalty given by $f_t(z) = \max(0, tz)$. The dashed lines depict both barrier and penalty functions when $t \rightarrow +\infty$.

4 EXPERIMENTS

Both the proposed log-barrier extension and the standard quadratic penalty in [15], i.e., $\mathcal{P}(f_i(S_\theta)) = [f_i(S_\theta)]_+^2$, are compatible with any differentiable function $f_i(S_\theta)$, including non-linear and fractional terms, as in Eqs. (8) and (9) introduced further in the paper. However, we hypothesize that our log-barrier extension is better for handling the interplay between multiple competing constraints. To validate this hypothesis, we compare both strategies on the joint optimization of two segmentation constraints related to region size and centroid. Furthermore, we included comparisons with a ReLU penalty, which parameterized by a gradually increasing t , in a way exactly similar to our log-barrier extension: $f_t(z) = \max(0, tz)$. Also, the ReLU penalty has a linear behaviour on the non-feasible set, similarly to our log-barrier extension. Therefore, a comparison with a gradually stricter ReLU on multiple constraints will confirm the importance of the barrier effect of our log-barrier extensions on the feasible set, which we discussed in the previous section. We will not compare directly to the Lagrangian optimization in [26] because the recent weakly supervised CNN segmentation results in [15] showed that a quadratic-penalty formulation of inequality constraints outperforms substantially the Lagrangian method in [26], in terms of performance and training stability. Therefore, we focus our comparisons on several penalties.

Region-size constraint: For a partially-labeled image, we define the size (or volume) of a segmentation for class k as the sum of its softmax predictions over the image domain:

$$\mathcal{V}_\theta^k = \sum_{p \in \Omega} s_{p,\theta}^k \quad (8)$$

Notice that we use the softmax predictions to approximate size because using the discrete binary values after thresholding would not be differentiable. In practice, we can make network predictions $s_{p,\theta}^k$ close to binary values using a large enough temperature parameter in the softmax function. We use the following inequality constraints on region size: $0.9\tau_{\mathcal{V}^k} \leq \mathcal{V}_\theta^k \leq 1.1\tau_{\mathcal{V}^k}$, where, similarly to the experiments in [15], $\tau_{\mathcal{V}^k} = \sum_{p \in \Omega} y_p^k$ is determined from the ground truth of each image⁶.

6. Since our focus is on evaluating and comparing constrained-optimization methods, we did not add additional processes to estimate the bounds without complete annotations of each training image. One can, however, use a single fully annotated training image to obtain such bounds or use an auxiliary learning to estimate region attributes such as size [14].

Region-centroid constraints: The centroid of the predicted region can be computed as a weighted average of the pixel coordinates:

$$\mathcal{C}_\theta^k = \frac{\sum_{p \in \Omega} s_{p,\theta}^k c_p}{\sum_{p \in \Omega} s_{p,\theta}^k}, \quad (9)$$

where $c_p \in \mathbb{N}^2$ are the pixel coordinates on a 2D grid. We constrain the position of the centroid in a box around the ground-truth centroid: $\tau_{\mathcal{C}^k} - 20 \leq \mathcal{C}_\theta^k \leq \tau_{\mathcal{C}^k} + 20$, with $\tau_{\mathcal{C}^k} = \frac{\sum_{p \in \Omega} y_p^k c_p}{\sum_{p \in \Omega} y_p^k}$ corresponding to the bound values associated with each image.

4.1 Datasets and evaluation metrics

Our evaluations and comparisons were performed on three different segmentation scenarios using synthetic, medical and color images. The data sets used in each of these problems are detailed below.

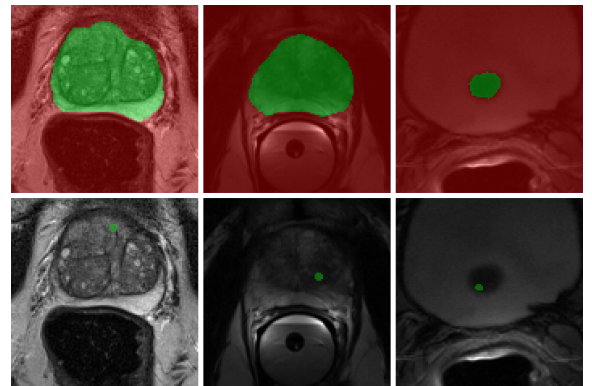


Fig. 2: Full mask of the prostate (*top*) and the generated point annotations (*bottom*). The background is depicted in red, and the foreground in green. No color means that no information is provided about the pixel class. The figures are best viewed in colors.

- **Synthetic images:** We generated a synthetic dataset composed of 1100 images with two different circles of the same size but different colors, and different levels of Gaussian noise added to the whole image. The target region is the darker circle. From these images, 1000 were

employed for training and 100 for validation; See Fig. 4, first column, for illustration. No pixel annotation is used during training ($\Omega_{\mathcal{L}} = \{\emptyset\}$). The objective of this simple dataset is to compare our log-barrier extension with several penalties in three different constraint settings: 1) only size, 2) only centroid, and 3) both constraints. For the first two settings, we expect both methods to fail since the corresponding segmentation problems are under-determined (e.g., size is not sufficient to determine which circle is the correct one). On the other hand, the third setting provides enough information to segment the right circle, and the main challenge here is the interplay between the two different constraints.

- **Medical images:** We use the PROMISE12 [17] dataset, which was made available for the MICCAI 2012 prostate segmentation challenge. Magnetic Resonance (MR) images (T2-weighted) of 50 patients with various diseases were acquired at different locations with several MRI vendors and scanning protocols. We hold 10 patients for validation and use the rest for training. As in [15], we use partial cross entropy for the weakly supervised setting, with weak labels derived from the ground truth by placing random dots inside the object of interest (Fig. 2). For this data set, we impose constraints on the size of the target region, as in [15].
- **Color images:** We also evaluate our method on the Semantic Boundaries Dataset (SBD), which can be seen as a scaling of the original PascalVOC segmentation benchmark. We employed the 20 semantic categories of PascalVOC. This dataset contains 11318 fully annotated images, divided into 8498 for training and 2820 for testing. We obtained the scribble annotations from the public repository of ScribbleSup [16], and took the intersection between both datasets for our experiments. Thus, a total of 8829 images were used for training, and 1449 for validation.

For the synthetic and PROMISE12 datasets, we resort to the common Dice index ($DSC = \frac{2|S \cap Y|}{|S| + |Y|}$) to evaluate the performance of tested methods. For PascalVOC, we follow most studies on this dataset and use the mean Intersection over Union (mIoU) metric.

4.2 Training and implementation details

Since the three datasets have very different characteristics, we considered a specific network architecture and training strategy for each of them.

For the dataset of synthetic images, we used the ENet network [24], as it has shown a good trade-off between accuracy and inference time. The network was trained from scratch using the Adam optimizer and a batch size of 1. The initial learning rate was set to 5×10^{-4} and decreased by half if validation performance did not improve for 20 epochs. Softmax temperature value was set to 5. To segment the prostate, we used the same settings as in [15], reporting their results for the penalty-based baselines. For PascalVOC, we used a Pytorch implementation of the FCN8s model [19], built upon a pre-trained VGG16 [31] from the Torchvision model zoo⁷. We trained this network with a batch size of 1 and a constant learning rate of 10^{-5} over time. Regarding

the weights of the penalties and log-barrier terms we investigated several values and we obtained the best performances with 10^{-4} and 10^{-2} , respectively.

For all tasks, we set to 5 the initial t value of our extended log-barrier (Algorithm 1). We increased it by a factor of $\mu = 1.1$ after each epoch. This strategy relaxes constraints in the first epochs so that the network can focus on learning from images, and then gradually makes these constraints harder as optimization progresses. The same scheduling is used for the ReLU baseline. Experiments on the toy example and PascalVOC were implemented in Python 3.7 with PyTorch 1.0.1 [25], whereas we followed the same specifications as [15] for the prostate experiments, employing Python 3.6 with PyTorch 1.0. All the experiments were carried out on a server equipped with a NVIDIA Titan V. The code is publicly available⁸.

4.3 Results

The following sections report the experimental results and comparisons on the three datasets introduced in Sec. 4.1.

4.3.1 Synthetic images

Results on the synthetic example for our log-barrier extensions and the penalty-based approaches are reported in Table 1. As expected, constraining the size only is not sufficient to locate the correct circle (2nd, 5th and 8th columns in Fig. 4), which explains the very low DSC values in the second column of Table 1. However, we observe that the different optimization strategies lead to very different solutions, with sparse unconnected dots for the penalty-based methods and a continuous shape for our log-barrier extension. This difference could be due to the high gradients of the penalty method in the first iterations, which strongly biases the network toward bright pixels. Constraining the centroid only locates the target region, but misses the correct boundaries (3rd, 6th and 9th columns in Fig. 4). Notice that for the centroid constraint, which corresponds to a difficult fractional term, our log-barrier yielded a much better performance than the penalties, with about 12% improvement over the quadratic penalty and 6% improvement over the parameterized ReLU penalty. The most interesting scenario is when both the size and centroid are constrained. In Fig. 3d, we can see that the penalty-based methods, both quadratic and ReLU with parameter t , are unstable during training, and have significantly lower performances than log-barrier extension; see the last column of Table 1. This demonstrates the barrier’s effectiveness in preventing predictions from going out of bounds (Fig. 1), thereby making optimization more stable. Notice that the gradually harder ReLU has the same performances and unstable behaviour as the quadratic penalty, which confirms the importance of the barrier effect when dealing with multiple constraints.

4.3.2 PROMISE12 dataset

Quantitative results on the prostate segmentation task are reported in Table 2 (*left* column). Without prior information, i.e., using only the scribbles, the trained model completely fails to achieve a satisfactory performance, with a mean Dice coefficient of 0.032. It can be observed that integrating the target size during training

7. <https://pytorch.org/docs/stable/torchvision/models.html>

8. https://github.com/LIVIAETS/extended_logbarrier

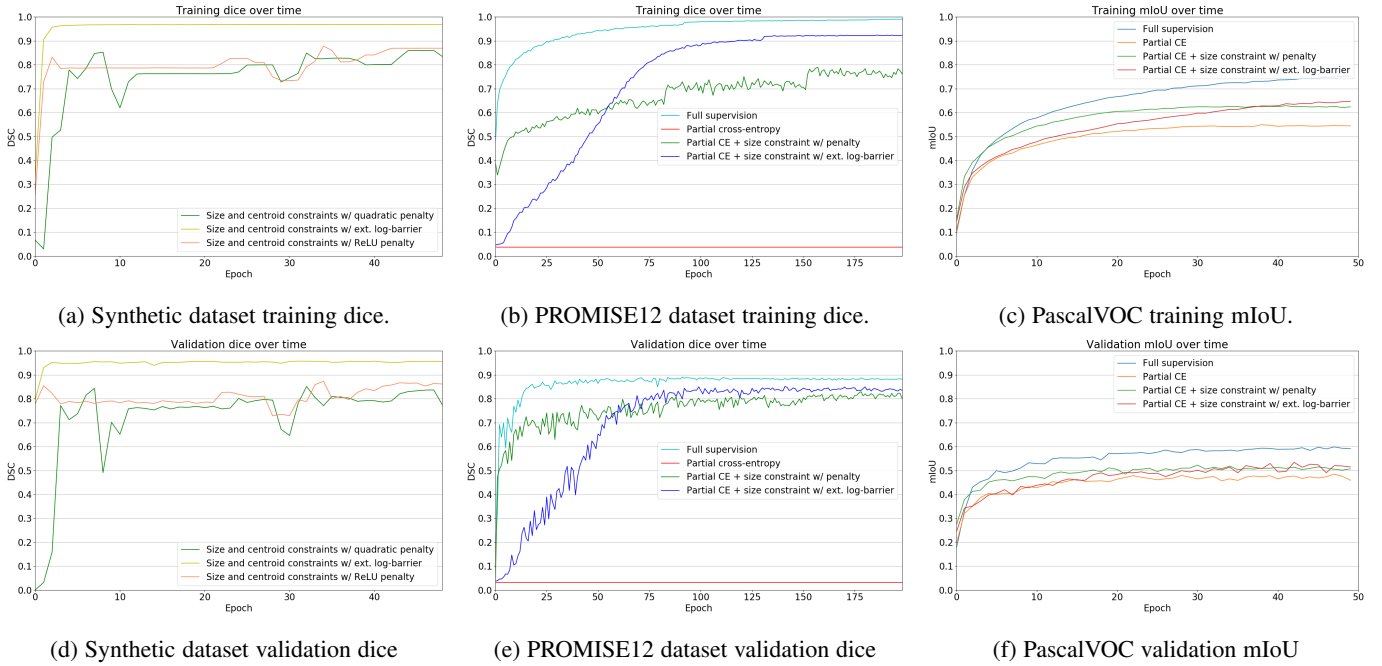


Fig. 3: Learning curves on the three data sets, for both the training and validation sets. Best viewed in colors.

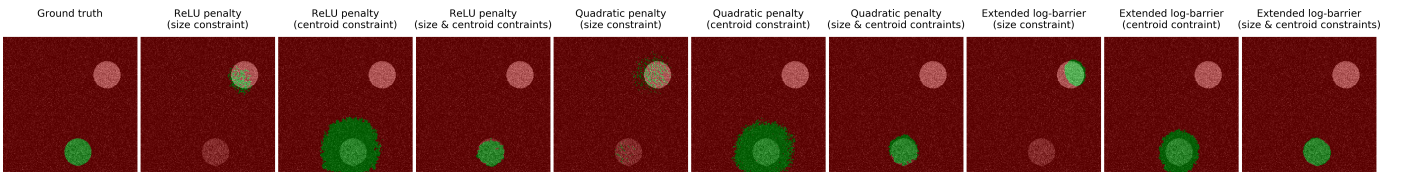


Fig. 4: Results of constrained CNNs on a synthetic example using the penalty-based methods and our log-barrier extension. The background is depicted in red, and foreground in green. Best viewed in colors.

Method	Constraints		
	Size	Centroid	Size & Centroid
ReLU penalty (w/ param. t)	0.0087	0.3770	0.8731
Quadratic penalty [15]	0.0601	0.3197	0.8514
Log-barrier extensions	0.0018	0.4347	0.9574

TABLE 1: Validation Dice on the synthetic example for several optimization methods and constraint settings.

significantly improves performance. While constraining the predicted segmentation with a penalty-based method [15] achieves a DSC value of nearly 0.83, imposing the constraints with our log-barrier extension increased the performance by an additional 2%. The use of log-barrier extensions to constrain the CNN predictions reduces the gap towards the fully supervised model, with only 4% of difference between both.

Method	Dataset	
	PROMISE12 (DSC)	VOC2012 (mIoU)
Partial cross-entropy	0.032 (0.015)	48.48 (14.88)
w/ quadratic penalty [15]	0.830 (0.057)	52.22 (14.94)
w/ extended log-barrier	0.852 (0.038)	53.40 (14.62)
Full supervision	0.891 (0.032)	59.87 (16.94)

TABLE 2: Mean and standard deviation on the validation set of the PROMISE12 and PascalVOC datasets when networks are trained with several levels of supervision.

4.3.3 PascalVOC

Table 2 (right column) compares the results of our log-barrier extension to those obtained with quadratic penalties and partial cross-entropy (i.e., using scribble annotations only), using region-size constraints. For reference, we also include the full-supervision results, which serve as an upper bound. From the results, we can see that the quadratic-penalty constraints improve the performances over learning from scribble annotations only by approximately 4%, in terms of mIoU. With the proposed log-barrier extension, the mIoU increases up to 53.4%, yielding a 1.2% of improvement over the quadratic penalty and only a 6.4% of gap in comparison to full supervision. The visual results in Fig. 6 show how the proposed framework for constraining CNN training helps reducing over-segmentation and false positives.

5 CONCLUSION

We proposed log-barrier extensions, which approximate Lagrangian optimization of constrained-CNN problems with a sequence of unconstrained losses. Our formulation relaxes the need for an initial feasible solution, unlike standard interior-point and log-barrier methods. This makes it convenient for deep networks. We also provided an upper bound on the duality gap for our proposed extensions, thereby generalizing the duality-gap result of standard log-barriers and showing that our formulation has dual variables that mimic implicitly (without dual projections/steps)

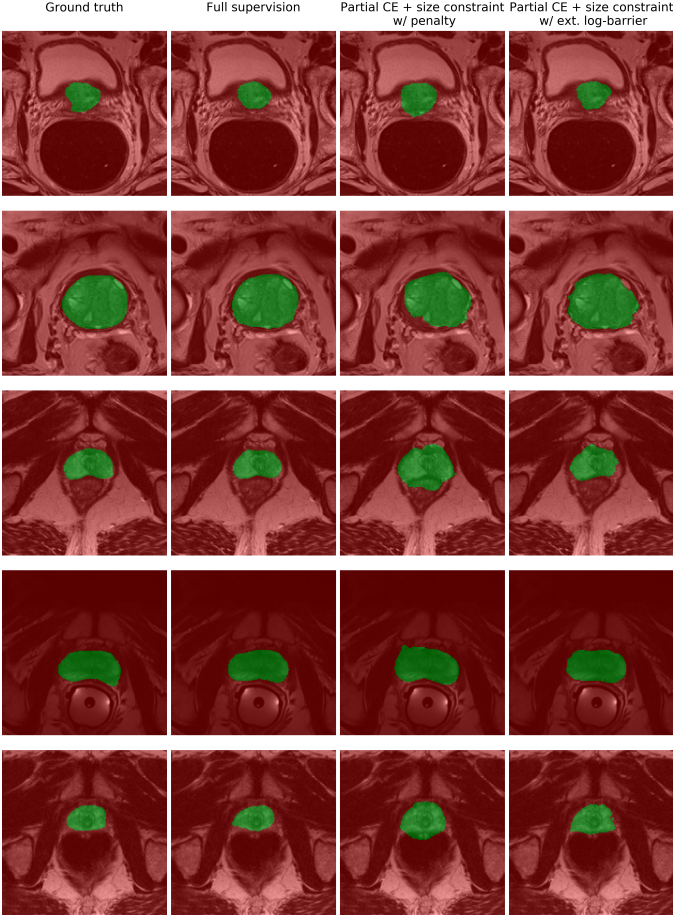


Fig. 5: Results on the PROMISE12 dataset. Images are cropped for visualization purposes. The background is depicted in red, and foreground in green. The figures are best viewed in colors.

Lagrangian optimization. Therefore, our implicit Lagrangian formulation can be fully handled with SGD, the workhorse of deep networks. We reported comprehensive constrained-CNN experiments, showing that log-barrier extensions outperform several types of penalties, in terms of accuracy and training stability.

While we evaluated our approach in the context of weakly supervised segmentation, log-barrier extensions can be useful in breadth of problems in vision and learning, where constraints occur naturally. This include, for instance, adversarial robustness [29], stabilizing the training of GANs [9], domain adaptation for segmentation [36], pose-constrained image generation [12], 3D human pose estimation [21], and deep reinforcement learning [11]. To our knowledge, for these problems, among others in the context of deep networks, constraints (either equality⁹ or inequality) are typically handled with basic penalties. Therefore, it will be interesting to investigate log-barrier extensions for these problems.

Since our focus was on evaluating and comparing constrained-optimization methods, we defined the constraints from prior knowledge about a few segmentation-region attributes (size and centroid). Such image-level attributes can also be learned from data using auxiliary regression networks, which could be useful in semi-supervision [14] and domain-adaptation [36] scenarios.

9. Note that our framework can also be used for equality constraints as one can transform an equality constraint into two inequality constraints.

It would interesting to investigate log-barrier extensions in such scenarios and with a much broader set of constraints, for instance, region connectivity or compactness, inter-region relationships and higher-order shape moments¹⁰.

APPENDIX A PROOF OF PROPOSITION 2

In this section, we provide a detailed proof for the duality-gap bound in Prop. 2. Recall our unconstrained approximation for inequality-constrained CNNs:

$$\min_{\theta} \mathcal{E}(\theta) + \sum_{i=1}^N \tilde{\psi}_t(f_i(S_{\theta})) \quad (10)$$

where $\tilde{\psi}_t$ is our log-barrier extension, with t strictly positive. Let θ^* be the solution of problem (10) and $\lambda^* = (\lambda_1^*, \dots, \lambda_N^*)$ the corresponding vector of implicit dual variables given by:

$$\lambda_i^* = \begin{cases} -\frac{1}{t f_i(S_{\theta^*})} & \text{if } f_i(S_{\theta^*}) \leq -\frac{1}{t^2} \\ t & \text{otherwise} \end{cases} \quad (11)$$

We assume that θ^* verifies approximately¹¹ the optimality condition for a minimum of (10):

$$\nabla \mathcal{E}(\theta^*) + \sum_{i=1}^N \tilde{\psi}'_t(f_i(S_{\theta^*})) \nabla f_i(S_{\theta^*}) \approx 0 \quad (12)$$

It is easy to verify that each dual variable λ_i^* corresponds to the derivative of the log-barrier extension at $f_i(S_{\theta^*})$:

$$\lambda_i^* = \tilde{\psi}'_t(f_i(S_{\theta^*}))$$

Therefore, Eq. (12) means that θ^* verifies approximately the optimality condition for the Lagrangian corresponding to the original inequality-constrained problem in Eq. (1) when $\lambda = \lambda^*$:

$$\nabla \mathcal{E}(\theta^*) + \sum_{i=1}^N \lambda_i^* \nabla f_i(S_{\theta^*}) \approx 0 \quad (13)$$

It is also easy to check that the implicit dual variables defined in (11) corresponds to a feasible dual, i.e., $\lambda^* > 0$ element-wise. Therefore, the dual function evaluated at $\lambda^* > 0$ is:

$$g(\lambda^*) = \mathcal{E}(\theta^*) + \sum_{i=1}^N \lambda_i^* f_i(S_{\theta^*}),$$

which yields the duality gap associated with primal-dual pair (θ^*, λ^*) :

$$\mathcal{E}(\theta^*) - g(\lambda^*) = -\sum_{i=1}^N \lambda_i^* f_i(S_{\theta^*}) \quad (14)$$

Now, to prove that this duality gap is upper-bounded by N/t , we consider three cases for each term in the sum in (14) and verify that, for all the cases, we have $\lambda_i^* f_i(S_{\theta^*}) \geq -\frac{1}{t}$.

- $f_i(S_{\theta^*}) \leq -\frac{1}{t^2}$: In this case, we can verify that $\lambda_i^* f_i(S_{\theta^*}) = -\frac{1}{t}$ using the first line of (11).
- $-\frac{1}{t^2} \leq f_i(S_{\theta^*}) \leq 0$: In this case, we have $\lambda_i^* f_i(S_{\theta^*}) = t f_i(S_{\theta^*})$ from the second line of (11). As t is strictly

10. Size and centroid are 0th and 1st shape moments.

11. When optimizing unconstrained loss via stochastic gradient descent (SGD), there is no guarantee that the obtained solution verifies exactly the optimality conditions.

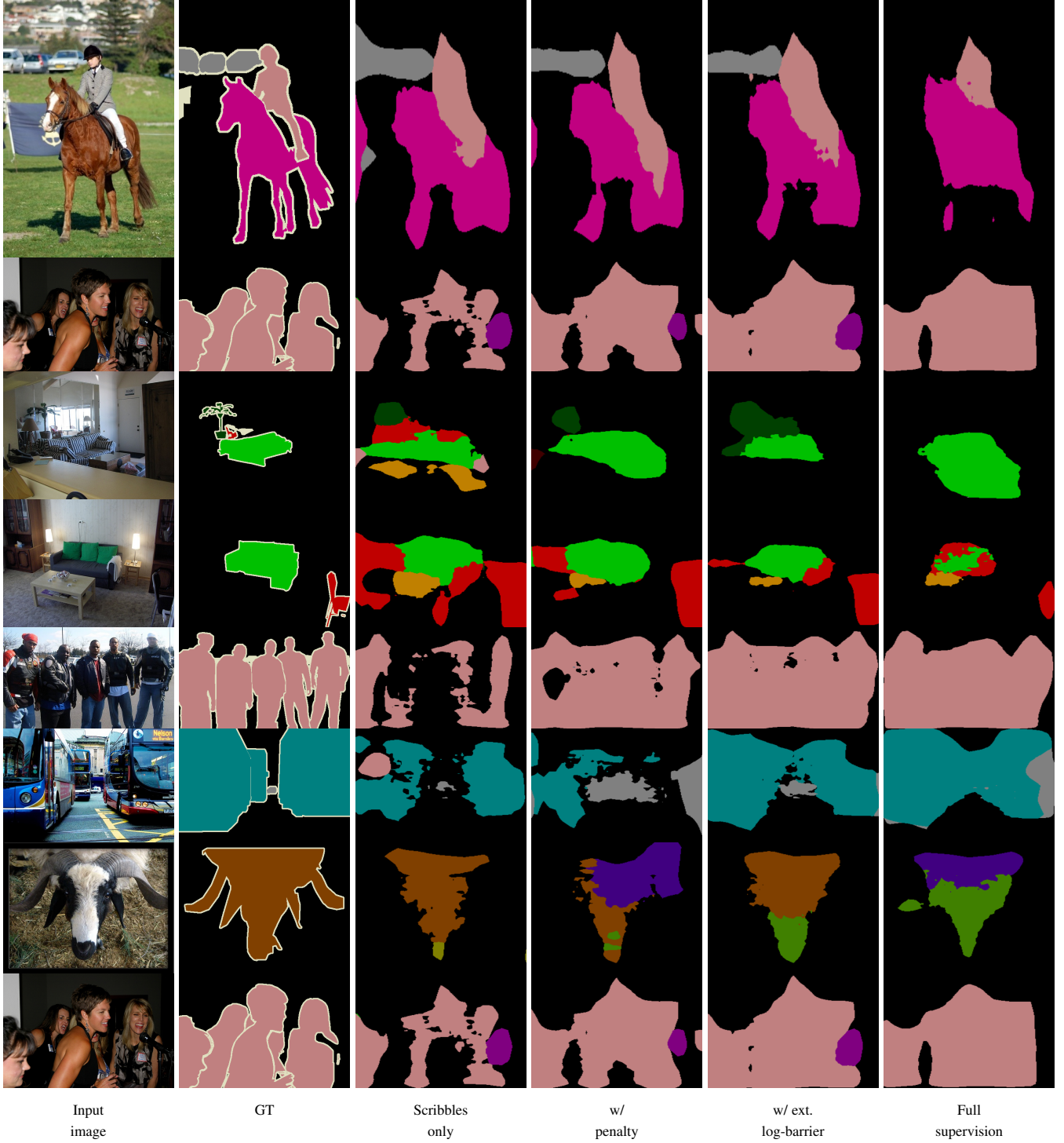


Fig. 6: Several visual examples on PascalVOC validation set. Best viewed in colors

positive and $f_i(S_{\theta^*}) \geq -\frac{1}{t^2}$, we have $tf_i(S_{\theta^*}) \geq -\frac{1}{t}$, which means $\lambda_i^* f_i(S_{\theta^*}) \geq -\frac{1}{t}$.

- $f_i(S_{\theta^*}) \geq 0$: In this case, $\lambda_i^* f_i(S_{\theta^*}) = tf_i(S_{\theta^*}) \geq 0 > -\frac{1}{t}$ because t is strictly positive.

In all the three cases, we have $\lambda_i^* f_i(S_{\theta^*}) \geq -\frac{1}{t}$. Summing this inequality over i gives $-\sum_{i=1}^N \lambda_i^* f_i(S_{\theta^*}) \leq \frac{N}{t}$. Using this inequality in (14) yields the following upper bound on the duality gap associated with primal θ^* and implicit dual feasible λ^* for

the original inequality-constrained problem:

$$\mathcal{E}(\theta^*) - g(\lambda^*) \leq N/t$$

□

This bound yields sub-optimality certificates for feasible solutions of our approximation in (10). If the solution θ^* that we obtain from our unconstrained problem (10) is feasible, i.e., it satisfies constraints $f_i(S_{\theta^*}) \leq 0$, $i = 1, \dots, N$, then θ^* is N/t -suboptimal for the original inequality constrained problem: $\mathcal{E}(\theta^*) - \mathcal{E}^* \leq N/t$. Our upper-bound result can be viewed as

a generalization of the duality-gap equality for the standard log-barrier function [3]. Our result applies to the general context of convex optimization. In deep CNNs, of course, a feasible solution for our approximation may not be unique and is not guaranteed to be a global optimum as \mathcal{E} and the constraints are not convex.

ACKNOWLEDGMENTS

This work is supported by the National Science and Engineering Research Council of Canada (NSERC), via its Discovery Grant program.

REFERENCES

- [1] A. L. Bearman, O. Russakovsky, V. Ferrari, and F. Li. What’s the point: Semantic segmentation with point supervision. In *European Conference on Computer Vision (ECCV)*, pages 549–565, 2016.
- [2] D. P. Bertsekas. *Nonlinear Programming*. Athena Scientific, Belmont, MA, 1995.
- [3] S. Boyd and L. Vandenberghe. *Convex Optimization*. Cambridge University Press, 2004.
- [4] R. Fletcher. *Practical Methods of Optimization*. John Wiley & Sons, 1987.
- [5] P. Gill, W. Murray, and M. Wright. *Practical Optimization*. Academic Press, 1981.
- [6] R. Girshick, J. Donahue, T. Darrell, and J. Malik. Rich feature hierarchies for accurate object detection and semantic segmentation. In *Conference on computer vision and pattern recognition*, pages 580–587, 2014.
- [7] I. Goodfellow, Y. Bengio, and A. Courville. *Deep learning*. MIT press, 2016.
- [8] L. Gorelick, F. R. Schmidt, and Y. Boykov. Fast trust region for segmentation. In *Conference on Computer Vision and Pattern Recognition (CVPR)*, pages 1714–1721, 2013.
- [9] I. Gulrajani, F. Ahmed, M. Arjovsky, V. Dumoulin, and A. C. Courville. Improved training of wasserstein gans. In *Neural Information Processing Systems (NIPS)*, pages 5767–5777, 2017.
- [10] M. Hardt, B. Recht, and Y. Singer. Train faster, generalize better: Stability of stochastic gradient descent. In *International Conference on Machine Learning (ICML)*, pages 1225–1234, 2016.
- [11] F. S. He, Y. Liu, A. G. Schwing, and J. Peng. Learning to play in a day: Faster deep reinforcement learning by optimality tightening. In *International Conference on Learning Representations (ICLR)*, pages 1–13, 2017.
- [12] Z. Hu, Z. Yang, R. Salakhutdinov, L. Qin, X. Liang, H. Dong, and E. P. Xing. Deep generative models with learnable knowledge constraints. In *Neural Information Processing Systems (NeurIPS)*, pages 10522–10533, 2018.
- [13] Z. Jia, X. Huang, E. I. Chang, and Y. Xu. Constrained deep weak supervision for histopathology image segmentation. *IEEE Transactions on Medical Imaging*, 36(11):2376–2388, 2017.
- [14] H. Kervadec, J. Dolz, E. Granger, and I. Ben Ayed. Curriculum semi-supervised segmentation. In *Medical Image Computing and Computer-Assisted Intervention (MICCAI)*, pages 1–8, 2019.
- [15] H. Kervadec, J. Dolz, M. Tang, E. Granger, Y. Boykov, and I. Ben Ayed. Constrained-cnn losses for weakly supervised segmentation. *Medical Image Analysis*, 2019.
- [16] D. Lin, J. Dai, J. Jia, K. He, and J. Sun. Scribblesup: Scribble-supervised convolutional networks for semantic segmentation. In *Conference on Computer Vision and Pattern Recognition (CVPR)*, pages 3159–3167, 2016.
- [17] G. Litjens, R. Toth, W. van de Ven, C. Hoeks, S. Kerkstra, B. van Ginneken, G. Vincent, G. Guillard, N. Birbeck, J. Zhang, et al. Evaluation of prostate segmentation algorithms for mri: the promise12 challenge. *Medical Image Analysis*, 18(2):359–373, 2014.
- [18] G. J. S. Litjens, T. Kooi, B. E. Bejnordi, A. A. A. Setio, F. Ciompi, M. Ghafoorian, J. A. W. M. van der Laak, B. van Ginneken, and C. I. Sánchez. A survey on deep learning in medical image analysis. *Medical Image Analysis*, 42:60–88, 2017.
- [19] J. Long, E. Shelhamer, and T. Darrell. Fully convolutional networks for semantic segmentation. In *Conference on Computer Vision and Pattern Recognition (CVPR)*, pages 3431–3440, 2015.
- [20] D. Marin, M. Tang, I. B. Ayed, and Y. Boykov. Beyond gradient descent for regularized segmentation losses. In *Computer Vision and Pattern Recognition (CVPR)*, pages 1–10, 2019.
- [21] P. Márquez-Neila, M. Salzmann, and P. Fua. Imposing Hard Constraints on Deep Networks: Promises and Limitations. In *CVPR Workshop on Negative Results in Computer Vision*, pages 1–9, 2017.
- [22] M. Niethammer and C. Zach. Segmentation with area constraints. *Medical Image Analysis*, 17(1):101–112, 2013.
- [23] G. Papandreou, L. Chen, K. P. Murphy, and A. L. Yuille. Weakly-and semi-supervised learning of a deep convolutional network for semantic image segmentation. In *International Conference on Computer Vision (ICCV)*, pages 1742–1750, 2015.
- [24] A. Paszke, A. Chaurasia, S. Kim, and E. Culurciello. Enet: A deep neural network architecture for real-time semantic segmentation. *arXiv preprint arXiv:1606.02147*, 2016.
- [25] A. Paszke, S. Gross, S. Chintala, G. Chanan, E. Yang, Z. DeVito, Z. Lin, A. Desmaison, L. Antiga, and A. Lerer. Automatic differentiation in pytorch. 2017.
- [26] D. Pathak, P. Krahenbuhl, and T. Darrell. Constrained convolutional neural networks for weakly supervised segmentation. In *International Conference on Computer Vision (ICCV)*, pages 1796–1804, 2015.
- [27] M. Rajchl, M. C. Lee, O. Oktay, K. Kamnitsas, J. Passerat-Palmbach, W. Bai, M. Damodaram, M. A. Rutherford, J. V. Hajnal, B. Kainz, et al. Deepcut: Object segmentation from bounding box annotations using convolutional neural networks. *IEEE Transactions on Medical Imaging*, 36(2):674–683, 2017.
- [28] S. N. Ravi, T. Dinh, V. Sai, R. Lokhande, and V. Singh. Constrained deep learning using conditional gradient and applications in computer vision. *arXiv:1803.0645*, 2018.
- [29] J. Rony, L. G. Hafemann, L. S. Oliveira, I. Ben Ayed, R. Sabourin, and E. Granger. Decoupling direction and norm for efficient gradient-based l2 adversarial attacks and defenses. In *Computer Vision and Pattern Recognition (CVPR)*, pages 1–10, 2019.
- [30] K. Simonyan and A. Zisserman. Two-stream convolutional networks for action recognition in videos. In *Neural Information Processing Systems (NeurIPS)*, pages 568–576, 2014.
- [31] K. Simonyan and A. Zisserman. Very deep convolutional networks for large-scale image recognition. In *International Conference on Learning Representations (ICLR)*, 2015.
- [32] M. Tang, A. Djelouah, F. Perazzi, Y. Boykov, and C. Schroers. Normalized Cut Loss for Weakly-supervised CNN Segmentation. In *Conference on Computer Vision and Pattern Recognition (CVPR)*, pages 1818–1827, 2018.
- [33] M. Tang, F. Perazzi, A. Djelouah, I. Ben Ayed, C. Schroers, and Y. Boykov. On Regularized Losses for Weakly-supervised CNN Segmentation. In *European Conference on Computer Vision (ECCV), Part XVI*, pages 524–540, 2018.
- [34] T. B. Trafalis, T. A. Tutunji, and N. P. Couellan. Interior point methods for supervised training of artificial neural networks with bounded weights. In *Network Optimization*, pages 441–470, 1997.
- [35] J. Weston, F. Ratle, H. Mobahi, and R. Collobert. Deep learning via semi-supervised embedding. In *Neural Networks: Tricks of the Trade*, pages 639–655. Springer, 2012.
- [36] Y. Zhang, P. David, H. Foroosh, and B. Gong. A curriculum domain adaptation approach to the semantic segmentation of urban scenes. *IEEE Transactions on Pattern Analysis and Machine Intelligence*, 2019.
- [37] Y. Zhou, Z. Li, S. Bai, C. Wang, X. Chen, M. Han, E. Fishman, and A. Yuille. Prior-aware neural network for partially-supervised multi-organ segmentation. In *International Conference on Computer vision (ICCV)*, pages 1–10, 2019.